

# Design of an Active Flapping Wing Mechanism and a Micro Aerial Vehicle using a single Rotary Actuator

Michael.A.A.Fenelon<sup>1</sup>, Tomonari Furukawa<sup>2</sup>

<sup>1</sup>Institute for Robotics and Intelligent Systems, Bangalore, India

<sup>2</sup>School of Mechanical and Manufacturing Engineering, The University of New South Wales, Sydney, Australia

mike28282@gmail.com

## Abstract

We present the design of an active flapping wing mechanism and a prototype micro aerial vehicle that generates four distinct flapping patterns. The mechanism, a modified slider-crank (MSC), operates using a single rotary actuator and generates active flapping and rotation of wings that are similar to the flight patterns of many flying creatures. The kinematics of the mechanism, flapping patterns, steering mechanisms and enhancements of the MSC mechanism were analyzed. The effectiveness of the mechanism has been demonstrated by developing a prototype of size 200mm x 200mm x 150mm and weighing 3.2grams with capability of constrained hover and forward flight using an external power supply.

**Keywords:** micro aerial vehicle, flapping wing, hover

## 1 Introduction

Recent years have seen the increasing popularity of micro aerial vehicles (MAVs) as their applications range from the military, surveillance, planetary exploration, search & rescue and many more. The Defence Advanced Research Projects Agency (DARPA) defines the MAV to be of a maximum size of 15cm in any direction. The majority of the research on MAVs have been conducted on minaturising existing flying machines such as airplanes and helicopters. Flapping wing crafts have substantial advantages over traditional flying crafts in criteria such as low noise signature, resonant operation, dynamic stall as a high-lift mechanism, high efficiency at smaller scales and low Reynold's number, survivable and robust [1,2].

Ornithopters are a class of flying craft that are designed based on bird flight. The past research developed various MAVs including the Microbat, the smallest electric ornithopter that successfully flew forwards [3]. The other projects include the University of Delaware's flapping wing MAV [4,5], Delfly and many commercial crafts, all of which similarly showed successful flights. However, multi-mode flying capabilities, such as hovering in addition to forward flight has not been effectively demonstrated. To create a flapping wing MAV that exhibits hovering, we look at some of nature's best flying and hovering creatures: dragonflies, hummingbirds and bees. The flapping patterns of these creatures consist of a flap or stroke and rotation or twisting of the wing, which

can be divided into two types of flapping wing mechanisms: active and passive. An active mechanism is the one in which wing rotation is generated by actively rotating the wing to generate an angle of attack during each stroke [6,7,8]. The Micromechanical Flying Insect at University of California, Berkeley generates such active wing flapping and rotation using four-bar mechanisms driven by two non-rotary actuators [9]. A passive mechanism uses aerodynamic drag and the flexibility of the wing to generate wing rotation; ornithopters come under this class. Unlike conventional flying crafts such as airplanes and helicopters which use aerodynamic lift to be airborne, dragonflies use aerodynamic drag to support approximately 76% of its weight [10]. The analysis of flapping wing motions of such creatures is crucial as they provide clues to design better flying machines at smaller scales in addition to increased efficiency.

This paper presents the design of an active flapping wing mechanism that replicates flapping patterns of dragonflies and a prototype MAV. Two steering mechanisms were demonstrated; differential steering and steering by altering the center of gravity of the prototype. The result of our design is a prototype capable of constrained hover and forward flight using an external power supply. The outline of the paper is as follows, Section 2 analysis the hovering patterns of dragonflies, Section 3 introduces and explains the operation of the MSC mechanism. Section 4 presents the kinematics of the mechanism and the simulation of flapping patterns. Section 5 presents the prototype's design and the implementation of two steering mechanisms. Sections 6 and 7 show the testing and results of the prototype respectively. Section 8 presents the conclusion and future work.

## 2 Analysis of Flight Patterns

The flapping patterns of dragonflies, hummingbirds and bees were analysed to extract key features that enable efficient flapping patterns to be incorporated into a prototype. Most hovering insects and hummingbirds use normal hovering: a symmetric flapping motion about the horizontal plane to generate enough vertical force to hover. However dragonflies and true hoverflies use asymmetric strokes along an inclined stroke plane [10,11], Figure 1. Vertical forces are generated during both half strokes in normal hovering while in asymmetric flapping the

majority of the vertical forces come from the downward stroke. Hovering along an inclined stroke plane is advantageous in comparison to normal hovering as 1) power is required for one half stroke only and 2) aerodynamic drag can be used to support weight. Studies show that in asymmetric flapping 76% of the vertical force comes from aerodynamic drag [10].

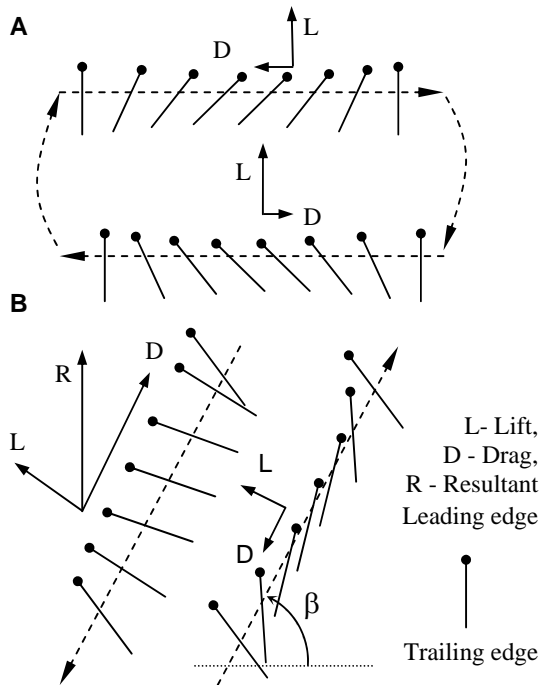


Figure 1 Hovering patterns, A: Normal hovering, stroke plane is parallel to the ground, B: Asymmetric flapping, hovering using an inclined stroke plane.

Using key features from flying creatures the MSC mechanism was designed such that efficient flapping patterns can be replicated. Figures 2 shows the MSC mechanism that is capable of generating four distinct flapping patterns using a single rotary actuator. The mechanism can also be viewed as a Four-Bar mechanism with the input and output linkages in orthogonal planes. The mechanism consists of a crank, coupler, drive-arm, pivot and main-arm spaced by specific distances. The coupler's design is crucial and consists of four rotational joints. The crank and the coupler form a rotational joint, the coupler and the drive-arm form a rotational joint. The crank, drive-arm and main-arm axes lie in the same plane: the stroke plane.

### 3 Operation of the MSC Mechanism

As the crank rotates it pushes or pulls the drive-arm along an arc (as the drive-arm is constrained by a pivot) creating wing strokes. The crank's rotation also inclines the coupler w.r.t the stroke plane. This inclination of the coupler twists or rotates the drive-arm and the wing. Hence wing flapping and rotation is achieved through the rotation of a crank.

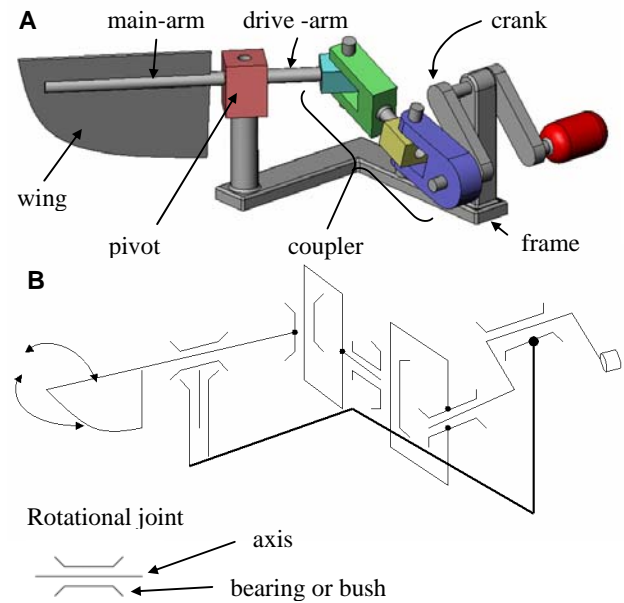


Figure 2 A: Modified Slider-Crank mechanism,

#### B: Kinematic diagram

The MSC mechanism was inspired from a Slider-Crank mechanism, but differs by 1) the slider (coupler – drive-arm joint) in the MSC mechanism moves along an arc as it is constrained by the pivot and 2) the coupler – drive-arm joint in the MSC is formed by a revolute joint whose axis is orthogonal to the drive-arm and coupler axis. In a normal Slider-Crank mechanism the coupler – slider joint is a rotational joint whose axis, if not in the same plane, is parallel to the crank axis. Hence the inclination of the coupler link in a normal Slider-Crank mechanism is nulled unlike in the MSC mechanism.

Reduction in components of the mechanism is crucial to building a light weight prototype. The coupler has four joints two of which can be replaced by a spherical joint, Figure 3. Prototypes using the mechanism were built with crank dimensions between 3mm and 5mm. Other components were also of the order of a few mm, at this size it was difficult to construct a rotational or a spherical joint along the length of the coupler. Hence flexible materials such as plastic and thin steel plates were used to form the coupler to allow for slight torsion and bending along the length of the coupler.

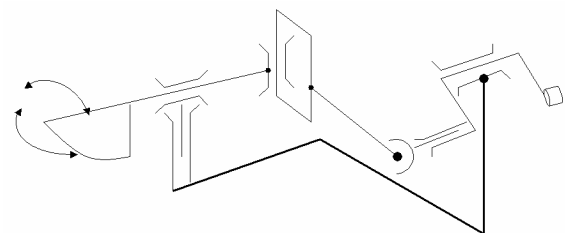


Figure 3 Kinematic diagram of the alternative MSC mechanism

## 4 Kinematics and Flapping Patterns.

The MSC mechanism is designed such that the transmission angle between each joint is symmetric during both strokes. Given the length of the crank ( $r_c$ ), desired maximum coupler inclination ( $\theta_c$ ) and maximum angle of swing or flapping ( $\theta_s$ ) that the mechanism has to generate, the dimension of each component and its spacing can be calculated, Figure 4. The kinematics analysis of the mechanism is done for the alternative MSC mechanism i.e. the coupler is rigid and of fixed dimensions.

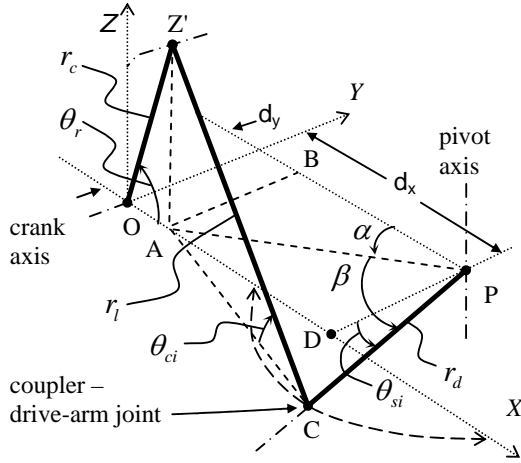


Figure 4 Kinematic analysis of the mechanism.

When  $\theta_r = 90^\circ$

$$r_l = r_c / \sin(\theta_c)$$

When  $\theta_r = 0^\circ$  and  $180^\circ$ , the coupler – drive-arm joint will lie on the XY plane at  $Y = 0$ ,  $X = r_c + r_l$  and  $X = r_l - r_c$  respectively. The value of  $\theta_{si}$  ranges between  $\pm \theta_s / 2$ . Hence the drive-arm length is given as,

$$r_d = r_c / \sin(\theta_s / 2)$$

The pivot distances ( $d_x, d_y$ ) are given as,

$$d_x = (r_l + r_c) - (r_d * \sin(\theta_s / 2))$$

$$d_y = r_d * \cos(\theta_s / 2)$$

Given the instantaneous position of the crank ( $r_c, \theta_r$ ) the position of the drive-arm ( $r_d, \theta_{si}$ ) can be calculated from triangle ABP.

$$OA = r_c * \cos(\theta_r)$$

$$\alpha = \text{acos}(BP/AP)$$

$$\theta_{ci} = \text{asin}(AZ'/r_l)$$

$$AC = r_l * \cos(\theta_{ci})$$

$$\beta = \text{acos}[(r_d^2 + AP^2 - AC^2) / (2 * r_d * AP)]$$

$$\theta_{si} = \alpha + \beta$$

Where  $\theta_{ci}$  &  $\theta_{si}$  are the instantaneous angles of the coupler and drive-arm respectively. The crank axis and the drive-arm axis lie in the same plane, the stroke plane. If either axis is moved along the Z axis the timing between each stroke can be adjusted and asymmetry can be achieved.

### 4.1 Flapping Patterns

The four distinct flapping patterns generated by the MSC mechanism arise by 1) changing the direction of crank rotation and 2) by including an offset angle ( $\theta_{off}$ ) between the coupler and the wing plane. A simulation of the flapping patterns is shown in Figures 5 & 6. These patterns are the projection of a chord of a rectangular wing as the crank rotation is incremented by  $10^\circ$ . Pattern 1, Figure 5, (A,B,C), is the primary flapping pattern of the MSC mechanism. It is generated by clockwise rotation of the crank and when  $\theta_{off} = 0^\circ$ . During the end of each stroke, the leading and trailing edges of the wing interchange which is not seen in flying creatures. Pattern 2 is obtained by adding an offset angle ( $\theta_{off}$ ) equal to the maximum coupler inclination ( $\theta_c$ ). This pattern is similar to hovering along an inclined stroke plane that is exhibited by dragonflies and hoverflies [10] except for the interchange of the leading and trailing edges. Pattern 3, Figure 6 (A,B,C), is identical to normal hovering exhibited by many of nature's fliers, this pattern is generated when the wing plane is normal to the coupler plane ( $\theta_{off} = 90^\circ$ ) and the crank rotation is opposite to that which is used to generate Pattern 1 & 2. Pattern 4 is generated by increasing the offset ( $\theta_{off} = 90^\circ + \theta_c$ ). In Pattern 3 & 4, it can be seen that the leading edge doesn't interchange at the end of each stroke, which implies that the leading edge vortex will be present during both strokes and will augment lift [12]. The flapping patterns were simulated for  $\theta_c = 30^\circ$ ,  $\theta_s = 90^\circ$ .

Two wing prototype MAVs were built such that the left and right halves had individual MSC mechanisms driven by a common shaft. The two cranks of the prototypes were in parallel planes so that there was zero phase difference between each half's flapping pattern. The flapping pattern is also determined by the position of the coupler – drive-arm joint. This joint can either be placed on the same or opposite side of the wing, Figure 7. The placement of this joint on the same side of the wing resulted in a significantly smaller and lighter prototype as compared to prior designs, Figure 8.

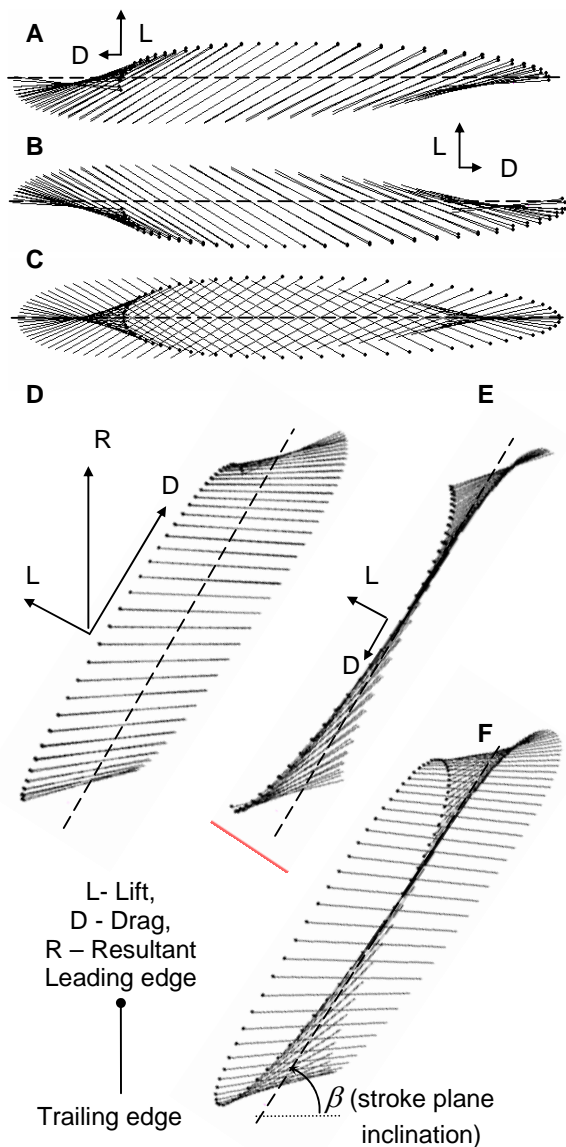


Figure 5 Flapping patterns, Pattern 1, A: Forward stroke, B: Backward stroke, C: Total pattern. Pattern 2, D: Down stroke, E: Upstroke, F: Total pattern.

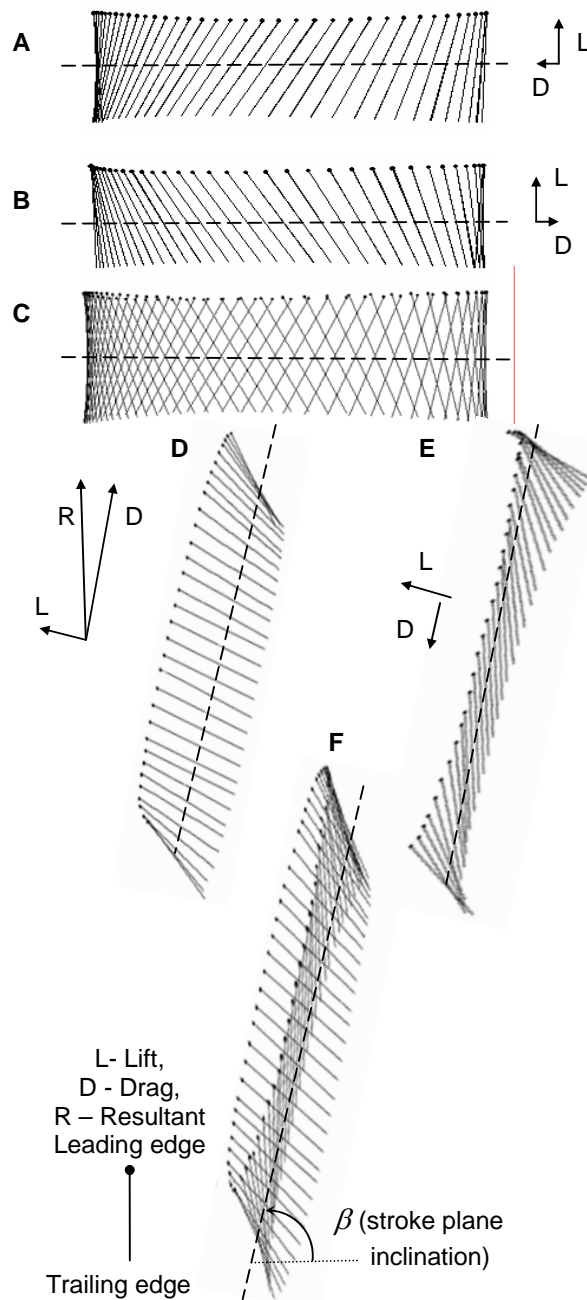


Figure 6 Flapping patterns, Pattern 3, A: Forward stroke, B: Backward stroke, C: Total pattern. Pattern 4, D: Down stroke, E: Upstroke, F: Total pattern

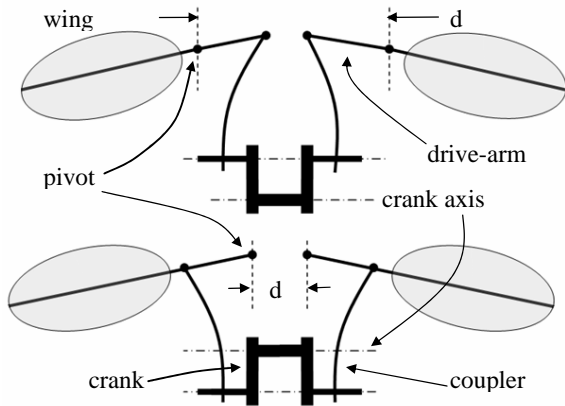


Figure 7 Positioning of the coupler – drive-arm joint.

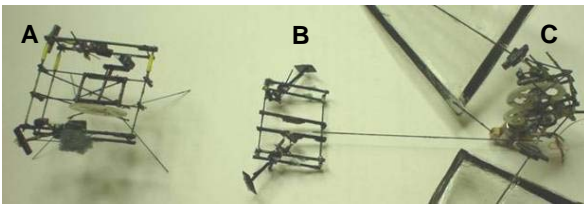


Figure 8 Comparison of prototypes, A & B were significantly larger and heavier in comparison to prototype C.

Table 1 Summary of parameters to generate respective flapping patterns (coupler – drive-arm joint is placed on the opposite side of the wing),  $\theta_a$  denotes the range of angle of attack that the wing will undergo.

	$\theta_{off}$	Crank rotation	Range of $\theta_a$
Pattern 1	Nil	cw	$-\theta_c$ to $\theta_c$
Pattern 2	$\theta_c$	cw	$0^\circ$ to $2\theta_c$
Pattern 3	$90^\circ$	acw	$90^\circ - \theta_c$ to $90^\circ + \theta_c$
Pattern 4	$90^\circ + \theta_c$	acw	$90^\circ$ to $90^\circ + 2\theta_c$

## 5 Prototype Flapping Wing MAV

A flapping wing MAV prototype, Figure 9 & 10, was built using twin MSC mechanisms driven by a single rotary actuator, a DC motor. The prototype, named CF 3, weighing 3.2grams, was designed for a crank length ( $r_c$ ) of 3mm, maximum coupler inclination ( $\theta_c$ ) of  $30^\circ$  and an angle of swing ( $\theta_s$ ) of  $90^\circ$ . The dimension of the coupler ( $r_l$ ) was 5.23mm, drive-arm ( $r_d$ ) = 4.24mm and offsets ( $d_x, d_y$ ) = 5.23mm, 3mm respectively. The prototype consists of two main halves, 1) frame A: supports the

wings and the twin MSC mechanisms and 2) frame B: houses the motor and gear 2. The prototype was designed such that frame A can rotate w.r.t frame B while maintaining meshing to drive the twin MSC mechanisms, variable inclination of the stroke plane was thus incorporated in the prototype.

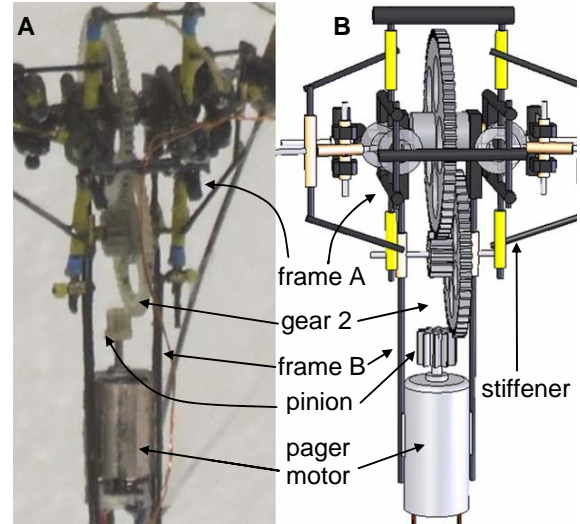


Figure 9 Prototype; A: CF3 prototype, B: CAD model of the CF3 prototype.

This prototype was constructed using 0.5mm, 1mm, 1.5mm carbon rods, 1mm and 1.5 mm brass tubes (inner diameter of 0.5mm and 1mm respectively) and 0.5mm stainless steel rods. The pivots were plastic tubes (3mm outer and 2mm inner diameter) with holes of 0.5mm drilled orthogonal to each other and the axis of the tube. The meshing between the pinion and gear 2 (both spur gears) is not ideal, but was enough to transmit power. The prototype uses a 6mm pager motor whose weight was reduced from 1.32 grams to 1.18 grams without compromising its performance characteristics by removing excess material from the motor housing. Stiffeners were used to confine the main-arm and drive-arm to the stroke plane as deviations occurred due to constructional imperfections and testing. A speed reduction ( $G$ ) of 23:1 was used in the prototype and the flapping frequency was calculated from the speed constant ( $K_v$ ) and the input voltage ( $V_{in}$ ) to the motor. The  $K_v$  of the pager motor is 3600rpm/V.

$$\text{Flapping frequency (Hz)} \quad f = (K_v * V_{in}) / (G * 60)$$

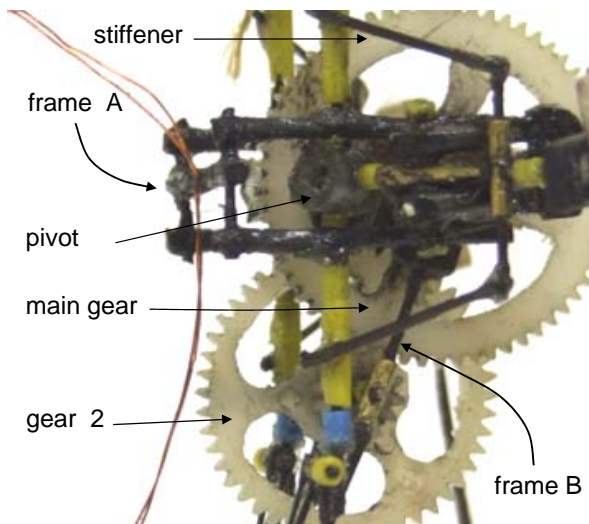


Figure 10 Details of the CF 3 prototype.

### 5.1 Steering Mechanisms

Two steering mechanisms were incorporated in the CF 3 prototype, 1) differential steering and 2) steering by altering the centre of gravity (CG) of the prototype. The rotation of frame A w.r.t frame B provides a means of steering the prototype; differential steering. The left and right halves of frame A are parallel to each other and have the same variable inclination w.r.t frame B. If these halves are made independent, then the left and right stroke planes can be inclined at different angles w.r.t frame B, Figure 11. Consider that the MAV hovers using any of the above flapping patterns, a slight inclination of the stroke plane will tilt the net vertical force forwards or backwards giving rise to a forward or backward lift component for each half. The tilt of the right and left stroke planes w.r.t frame B ( $d\theta_r$  &  $d\theta_l$ ) determine the forward or backward lift components. As each independent stroke plane is tilted a phase difference arises between the left and right flapping patterns since either flapping pattern advances or lags w.r.t the other. It is assumed that sufficient vertical force is present to maintain hovering while imparting other maneuvers.

Another steering mechanism was incorporated in the prototype; steering by altering the CG. The CG was altered by moving the position of the motor in X & Y directions using a two axes gimbal while maintaining meshing between respective gears, Figure 12. Power transmission from the motor through the gimbal and to the twin MSC mechanisms was done using a combination of an idler gear and gear 2. Axis 1 passes through the mesh between the idler and gear 2, axis 2 is the axis of gear 2.

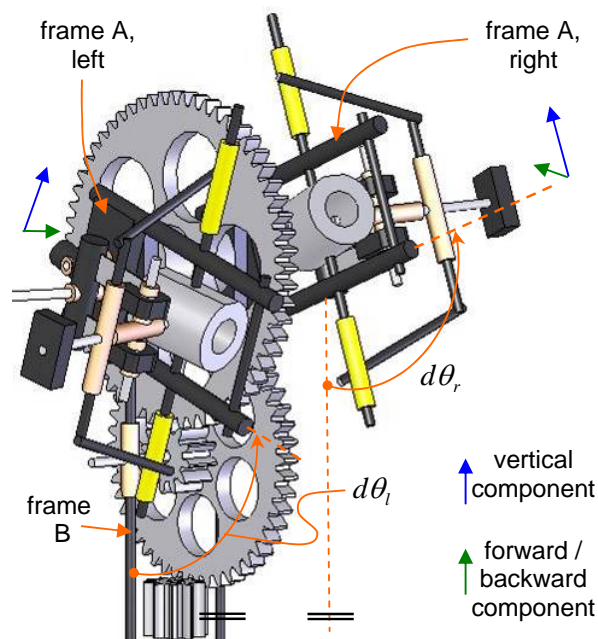


Figure 11 Differential steering by altering individual stroke planes to create a forward or backward lift component - reword.

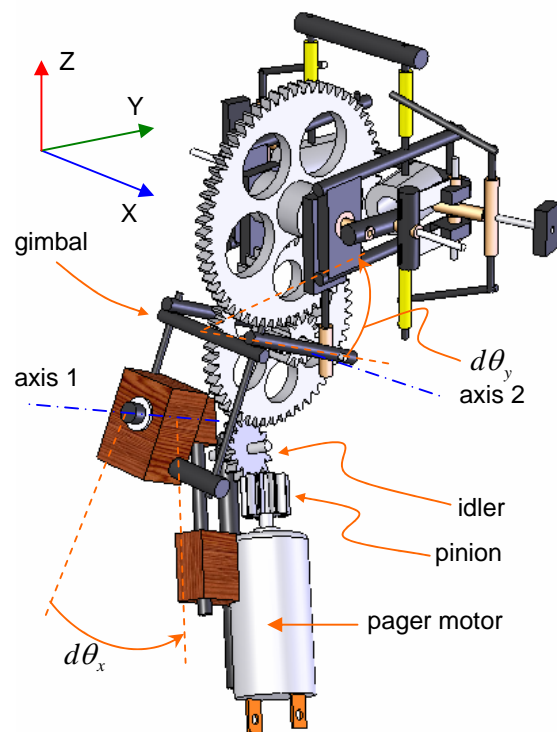


Figure 12 Steering by altering the CG of the prototype

The idler (spur gear) is not the best option for power transmission in this design, it was chosen due to weight constraints over other alternatives such as bevel, crown, worm gears etc or their combinations. A two axis gimbal was redundant as frame A could already rotate w.r.t frame B, hence only one axis (axis 1) is needed to shift the CG in the X direction. However, to incorporate both steering mechanisms a two axis gimbal is required in addition to

having frame A rotate w.r.t frame B. No actuators were added to incorporate either steering mechanism in the final prototype although experimentation was carried out using shape memory alloys.

## 6 Testing

Testing was done using a simple set up to observe differences in vertical force generation determined by flapping patterns and wing characteristics, Figure 13. The prototype was attached to one end of a 1mm carbon fibre (CF) rod (~50cm in length) and suspended in air with a pointer against a ruler. The flexing of the carbon fiber rod is advantageous as any small vertical force generated by the pototype moves the pointer significantly. Figures 14 to 16 show the results of tests on the CF 3 prototype. Figure 14 shows the relative vertical force exhibited by the prototype using flat and cambered wings using flapping pattern 1. The wing was oval in shape, span of 6.5cm, its periphery made of 0.5mm CF and the wing surface covered with a mylar sheet (0.005mm thick). The wing chord was gradually reduced to impart camber into the wing. Figure 15 shows the difference in relative vertical force between flapping pattern 1 & 3 using the prior oval wings. Figure 16 shows the difference between symmetric and asymmetrical rectangular wings (6cm wing span and 4cm chord length) using flapping pattern 3.

Tests using flapping patterns 2 & 4 produced large oscillations as the beat frequency was rather low. Although the oscillations decreased with increase in flapping frequency there were substantial oscillations and the results could not be quantified. One reason for this behavior could be the difference in drag components during the up and down strokes. Since  $\theta_c = 30^\circ$ , the drag component during the up-stroke would result in a significant downward force. It is unclear whether the oscillations were due to aerodynamic drag or effects of the wing's momentum.

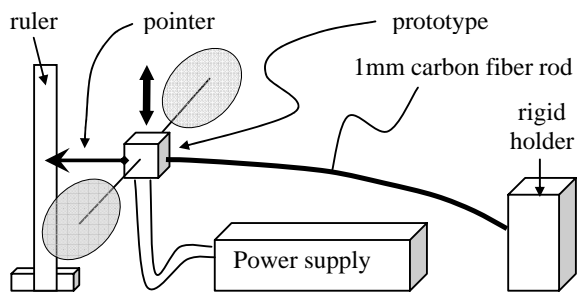


Figure 13 Set up to observe relative vertical forces based on flapping patterns and wing characteristics.

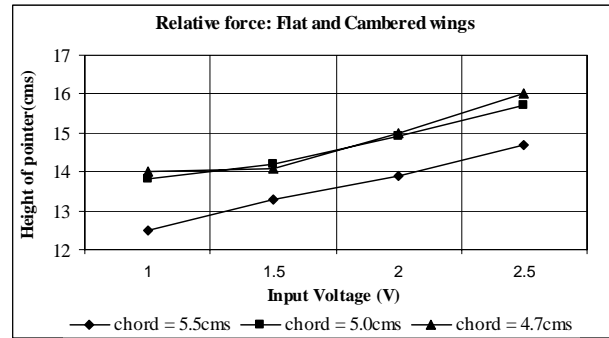


Figure 14 Comparing the relative vertical force between flat and cambered wings using flapping pattern 1.

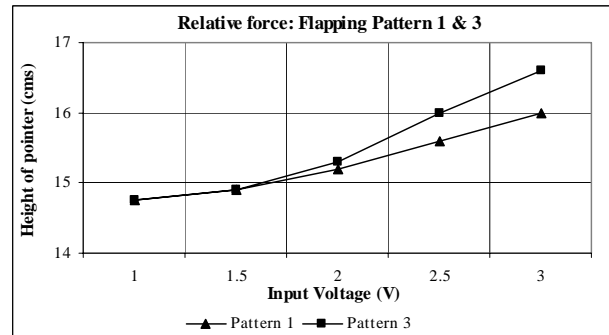


Figure 15 Comparison of flapping patterns 1 & 3.

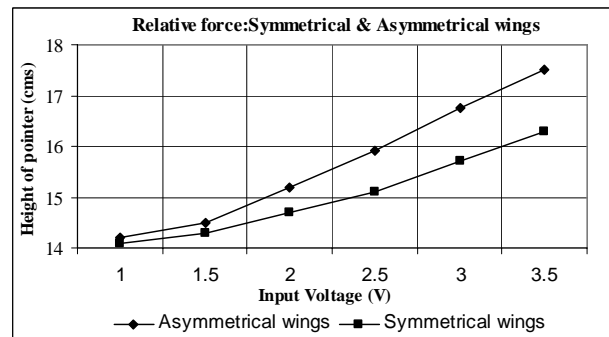


Figure 16 Plot comparing the net vertical force between symmetric & asymmetric wings (wing symmetry about the stroke plane was considered).

## 7 Results

Using the above results, the CF 3 prototype was fitted with an asymmetric pair of tapered wings (span of 9cm and inner rib of 6cm) and tested on a simple balance. The prototype was found to hover using flapping pattern 3 with an external power supply of 3.4V at 190mA,  $f = 8.8\text{Hz}$ . A significant load of 0.92grams (a Lithium Polymer battery) was attached to the body of the prototype and tested for hovering capability. The prototype continues to exhibit hovering with an increased external input of 4.4V at 220mA,  $f = 11.5\text{Hz}$ . Unconstrained tests were conducted by suspending the prototype using a string and powering it externally, the prototype was unstable and unable to hover even for a short span. Four passive flaps

were added to stabilise the prototype and achieve hover and forward flight, Figure 17.

## 8 Conclusion

This paper presented a mechanism that generates active flapping whose patterns are modeled on dragonflies. The proposed and tested mechanism generates four distinct flapping patterns using a DC motor. Twin MSC mechanisms were incorporated into a two winged MAV prototype that exhibits constrained hovering and forward flight, weighs 3.35grams (3.2grams excluding the four flaps) and measures 200mm x 200mm x 150mm. The prototype also exhibits the usage of aerodynamic drag for hovering, differential steering and steering by altering the centre of gravity of the prototype. The prototype and its design indicates that the MSC mechanism is a good solution for flapping wing MAVs. Future work will focus on measurement of vertical forces, better wing designs, usage of optimum flapping patterns, control and stabilisation.

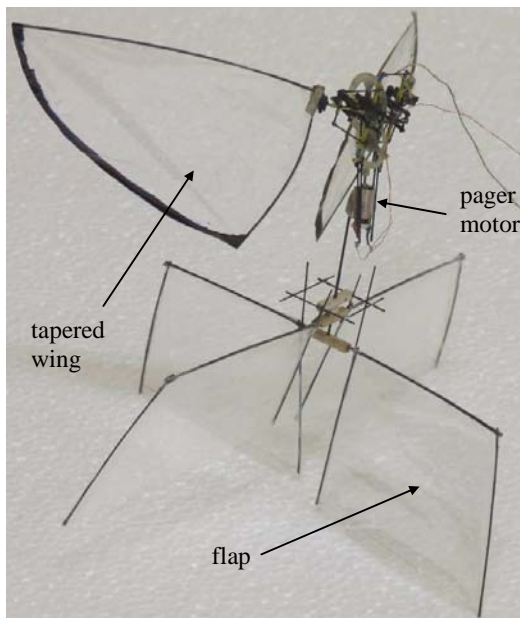


Figure 17 Final flapping wing prototype MAV.

## Acknowledgement

This work was partly supported by the ARC Centre of Excellence program, funded by the Australian Research Council (ARC) and the New South Wales State Government. We thank the Computational Mechanics and Robotics group, UNSW. We also thank Director IRIS and CAIR, DRDO.

## References

- [1] "Planetary Exploration Using Biomimetics An Entomopter for Flight on Mars," Phase II Final Report, NASA Institute for Advanced Concepts Project NAS5-98051, October 2002.
- [2] J. D. DeLaurier, "An aerodynamic model for flapping-wing flight," *Aeronaut.J.*, vol. 97, no. 964, pp. 125-130, Apr. 1993.
- [3] Microbat: A Palm-Sized Electrically Powered Ornithopter, TN Pornsin, YC Tai, M Keennon
- [4] Zaeem A. Khan, Sunil K. Agrawal, "Design of Flapping Mechanisms Based on Transverse Bending Phenomena in Insects", IEEE International Conference on Robotics and Automation, Orlando, Florida, 2006.
- [5] Rajkiran Madangopal, Zaeem A Khan, Sunil K Agrawal, "Energetics based design of small flapping wing air vehicles", International Conference for Robotics and Automation, 2004, VOL. 11, NO. 4.
- [6] Sean H. McIntosh, Zaeem A. Khan, Sunil K. Agrawal, "Design of a Mechanism for Biaxial Rotation of a Wing for a Hovering Vehicle", IEEE/ASME TRANSACTIONS ON MECHATRONICS, 2006, VOL. 11, NO. 2.
- [7] Galinski, C., & Zbikowski, R., 2005 Insect-like flapping wing mechanism based on a double spherical Scotch yoke. *Journal of the Royal Society: Interface* Vol 2, No 3, pp. 223-235, June 22 2005.
- [8] Zbikowski, R., Galinski, C., & Pedersen, C. B., 2005a Four-bar linkage mechanism for insect-like flapping wings in hover: Concept and an outline of its realisation. *Transactions of the ASME: Journal of Mechanical Design* Vol 127, No 4, pp. 817-824, Jul 2005.
- [9] Wing Transmission for a Micromechanical Flying Insect, R.S. Fearing, K.H. Chiang, M. Dickinson, D.L. Pick, M. Sitti, and J. Yan, IEEE Int. Conf. on Robotics and Automation, April, 2000.
- [10] Z. Jane Wang, The role of drag in insect hovering, *J. Expr. Bio.* 207, 4147-4155 (2004)
- [11] Z. Jane Wang, Dissecting Insect Flight, *Annu. Rev. Fluid Mech.* 2005.37, 183-210 (2005)
- [12] Wilmott, A.P., Ellington, C.P., and Thomas, A.L.R., "Flow Visualization and Unsteady Aerodynamics in the Flight of the Hawk Moth *Manduca sexta*," *Philosophical Transactions of the Royal Society B*, Vol 352, 1997, pp. 303-316.